Anisotropic ionic transport in quartz: the effect of twin boundaries

2001 J. Phys.: Condens. Matter 13 9445

(http://iopscience.iop.org/0953-8984/13/42/305)

INSTITUTE OF PHYSICS PUBLISHING JOURNAL OF PHYSICS: CONDENSED MATTER

J. Phys.: Condens. Matter **13** (2001) 9445–9454 PII: S0953-8984(01)26975-6

Anisotropic ionic transport in quartz: the effect of twin boundaries

Mark Calleja[1], **Martin T Dove and Ekhard K H Salje**

Mineral Physics Group, Department of Earth Sciences, University of Cambridge, Downing Street, Cambridge CB2 3EQ, UK

E-mail: mcal00@esc.cam.ac.uk (Mark Calleja)

Received 19 July 2001
Published 5 October 2001
Online at stacks.iop.org/JPhysCM/13/9445

Abstract

Transport of Na^+ and Li^+ under the influence of an electric field in twinned quartz is simulated using molecular dynamics techniques. Comparison between bulk transport and transport along twin boundaries shows that the cations are trapped inside twin walls for weak fields along the crystallographic *c*-axis. Stronger fields lead to transport along twin walls with significantly lower mobility than in the bulk. With $\boldsymbol{E}$ along [110], transport in the wall is faster than in the bulk. We observe cation trapping preferentially in the twin walls when $\boldsymbol{E}$ is applied out of the plane of the wall.

1. Introduction

It is a well-established concept that ionic transport along grain boundaries is very different from transport in bulk material [1, 2]. It was found that high-angle boundaries can lead to higher mobilities because favourable trajectories exist either in or near the boundary. In other cases, transport can be reduced because the interfacial region contains additional trapping centres. In addition, ionic transport often leads to space-charge phenomena, which also influence the overall mobility.

Similar features were recently observed experimentally in (ferroelastic) twin boundaries [3]. Typical examples are the enhanced transport of oxygen [4] or sodium [5] along twin walls in ferroelastic WO_3. Similarly twin walls and antiphase boundaries can act as trapping centres with significant enrichment of atomic species along these internal interfaces. Examples are the enrichment of antiphase boundaries in NiAl alloys with Cr [6], the enrichment with alkali ions and depletion of Ca and Al in the mineral anorthoclase (Na, K)$AlSi_3O_8$ [7] which explains the strong memory effect in these materials [8]. Shallow Pb^{3+} hole traps in PZT may also be related to the occurrence of twin walls [9].

[1] Author to whom any correspondence should be addressed. Telephone: +44 (0) 1223 333373; Web site: http://www.esc.cam.ac.uk/minsci.

The importance of such observations is twofold. Firstly, twin boundaries in ferroelastic materials can be generated by external stresses or specific thermal treatment in order to engineer fast diffusion or trapping trajectories in device applications [10–14], with junction-type needle configurations as a characteristic feature [15]. Diffusion into twin boundaries is facilitated by trapping centres at the junction between the surface and the twin wall [16]. Secondly, cation-ordering processes during structural phase transitions can be kinetically enhanced by interfacial transport; see e.g. [17] and references given there. Similar effects also exist in displacive transitions where interfacial movements can accelerate the transition process [18].

It is the purpose of this paper to use one of the most simple cases of Dauphiné-type twin boundaries in quartz as a prototype of a co-elastic twin boundary and identify the transport mechanisms related to these boundaries. As transport in electric fields is easily observed for Na^+ and Li^+, we have chosen these elements as traces in our model simulations. Quartz is a convenient example because its phase transition $\beta \rightarrow \alpha$ (622 $\rightarrow$ 32) near 847 K has been thoroughly studied (see e.g. [19] and references given there) while the nature of the Dauphiné twinning is also well known [20, 21]. Furthermore, reliable empirical potentials were derived by van Beest and co-workers [22], so it proved relatively simple to simulate the local structural features of the twin walls. We show in this paper that the *c*-axis channels in quartz are heavily distorted inside the wall, leading to trapping within and slow diffusion along these channels. Side channels perpendicular to the crystallographic *c*-axis were less distorted and transport along [110] is enhanced within the twin boundary

2. Simulation details

2.1. Simulation method

The investigative method chosen here is that of empirical-potential molecular dynamics. The nature and scale of the systems studied here ($\sim 10^4$ ions) precluded the use of more accurate, but computationally expensive, *ab initio* techniques. Indeed, due to the timescales involved we study forced diffusion, namely diffusion in the presence of a strong applied electric field (which is one of the standard external potentials available within DL_POLY [23], the package employed here).

We used a thin quartz configuration comprising 7260 tetrahedra ($22 \times 22 \times 5$ unit cells), with parallelepiped periodic boundary conditions. All simulations were performed in the isothermal–isobaric (NPT) ensemble. The time step for all simulations was 7.5×10^{-4} ps.

The interatomic potentials used here are simple two-body Buckingham potentials with partial ionic charges, and have the following functional form for ions i and j separated by distance r:

$$V(r) = A_{ij} \exp(-b_{ij} r) - \frac{C_{ij}}{r^6} + \frac{q_i q_j}{r}. \tag{1}$$

We used the parameters due to van Beest and co-workers where available [22], but generated our own Li–O interaction parameters by fitting to the alpha-spodumene structure ($LiAlSi_2O_6$) given in [24] using GULP [25]. The fitted Li–O interaction resulted in the relaxed spodumene lattice constants varying by less than 1% from the experimental data, and the unit-cell angle for this monoclinic structure changing by 1.1%, as shown in table 1 below. Most Si–O and Al–O bond lengths changed by $\sim$1%, though one particular Al–O bond changed by 5.9%. Within the spirit of the empirical-potential methods used here, we considered this level of fit acceptable for the calculations employed in this work.

The parameters used here are given in table 2. A cut-off of 10 Å on the non-coulombic interactions was employed.

Table 1. Experimental and fitted values for the lattice constants of alpha-spodumene (in Å).

	a	b	c	θ
Experimental value	9.462	8.392	5.221	110.18°
Fitted value	9.540	8.454	5.191	108.97°

Table 2. Potential parameters used in this work.

Interaction	A_{ij} (eV)	b_{ij} (Å^{-1})	C_{ij} (eV Å^6)	Charge q
O–O	1388.773	2.76	175.0	$q_{\mathrm{O}} = -1.2$
Si–O	18003.7572	4.87318	133.5381	$q_{\mathrm{Si}} = 2.4$
Al–O	16008.5345	4.79667	130.5659	$q_{\mathrm{Al}} = 1.4$
Na–O	3542.2072	4.13455	0.0	$q_{\mathrm{Na}} = 1.0$
Li–O	1149.4126	3.5652	0.0	$q_{\mathrm{Li}} = 1.0$

2.2. Domain wall formation

Our starting point was a uniform β-quartz configuration which was then run at temperatures below the transition temperature. This allowed the sample to undergo a phase transition, and domain walls were observed to form. An example of a twin wall formed using this approach at 10 K is shown in figure 1, which depicts the silica tetrahedra viewed along the c-axis. Note the shearing evident at the domain wall, which is necessary to preserve the tetrahedral integrity. The walls can be located by measuring a relevant order parameter that is zero in the high-symmetry phase but appears on entering the low-symmetry phase. A suitable candidate for this purpose is the tetrahedral tilt angle with respect to the c-axis. This is due to the rotation

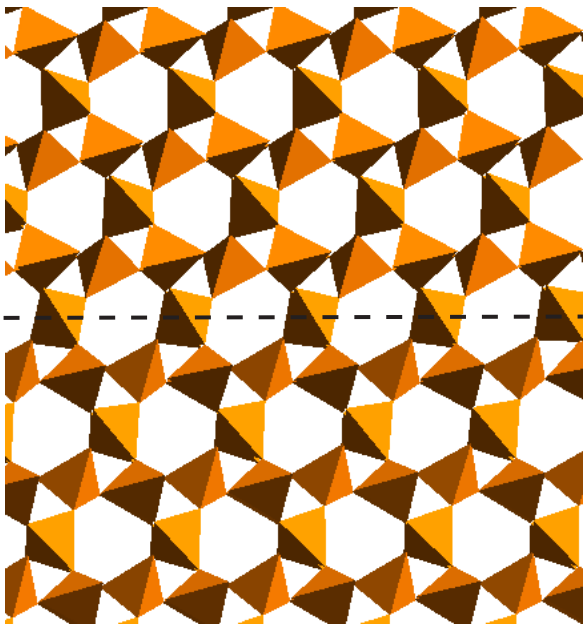

Figure 1. The domain wall (along the dashed line) in quartz at $T = 10$ K, viewed along [001]. (This figure is in colour only in the electronic version)

of the relatively rigid tetrahedra on undergoing the displacive transition [26]. Figure 2 shows a plot of this parameter for $T = 10$ K. Note how the tilt angle goes to zero at the walls, with a wall thickness of ∼13 Å. This would appear to be comparable, if on the low side, to values deduced experimentally for other materials (e.g. the low-temperature limit for domain walls in $LaAlO_3$ is ∼40 Å) [27].

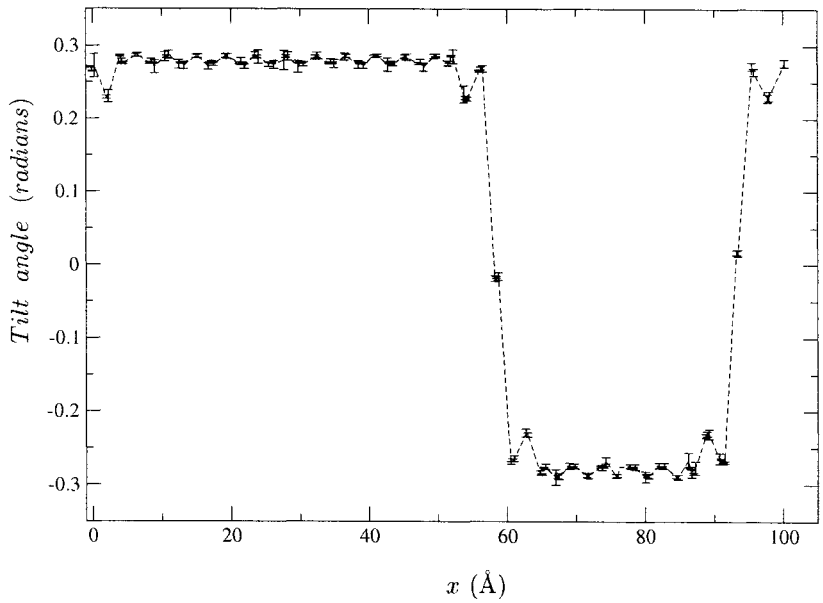

Figure 2. Order parameter (i.e. tetrahedral tilt angle made with the *c*-axis) plotted perpendicular to the domain wall at $T = 10$ K. Note that the line connecting the simulation data is drawn merely as a visual aid.

At this low temperature one can discern small-amplitude oscillations on the bulk value of the order parameter. Ripples in the bulk value of the order parameter have been calculated by Houchmanzadeh *et al* using a simple model which utilizes harmonic potentials between layers of atoms [28]. These authors also find that the amplitude of the ripples becomes larger as one approaches the transition temperature. However, as one increases the system temperature within the MD simulation, this rippling becomes hard to measure accurately due to the pronounced thermal excitation of the tetrahedra, although the effect is still discernible. The empirical potentials used in this study result in a wall energy of 9.5×10^{-2} J m^{-2} in the $T \to 0$ K limit. This value was calculated by comparing the potential energies of the twinned and untwinned crystal, and is comparable to the values calculated for perovskite structures using Landau–Ginzburg theory [29].

2.3. Simulation of diffusion

To study diffusion, we introduce alkali cations at various points within the crystal structure. Charge neutrality in the system was achieved by replacing a required number of silicon cations in the bulk region by aluminium cations at random positions. Specifically, ten alkali cations were inserted into the sample: five in the bulk and five within the domain walls. An external electric field was then applied to the system along various directions in order to determine the relative mobilities of the cations in the two different environments. Indeed, the technique of

applying an electric field to a quartz crystal is used in industry to sweep interstitial impurities from within crystals to the surface [30]. After a simulation was deemed to be thermally equilibrated, statistics were gathered over periods of ∼10 ps.

3. Results

3.1. Transport along [001]

Our first results are for $\boldsymbol{E}$ applied along [001] with Na^+ cations (note that we quote $\boldsymbol{E}$ in units of 10^8 V cm^{-1}). We studied two temperatures, namely 300 K and 700 K. A plot for the average cation velocity along [001] is shown in figure 3. Note that due to the time periods accessible to the simulations (∼10^{-11} s), correspondingly large field strengths were applied in order to produce discernible ionic conductivity (∼10^7 V cm^{-1}). Such large fields were necessary to overcome the potential barrier separating adjoining cavities in the quartz structure within such short timescales. This can be compared with [31], where fields of the order of 10^4 V cm^{-1} were used to study effects measured over hours.

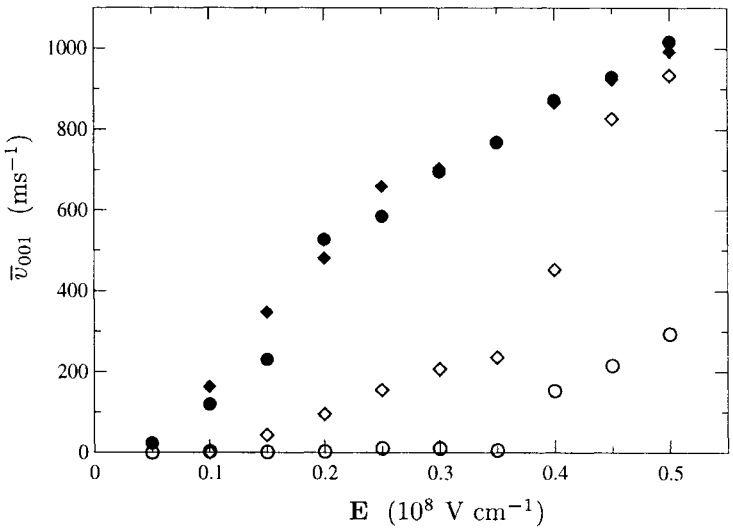

Figure 3. Average velocity along the c-axis for Na^+ ions with $\boldsymbol{E}$ applied along [001]. Note that circles refer to data at $T = 300$ K while diamonds are for $T = 700$ K; filled symbols are for cations in the bulk while empty symbols are for cations in the walls.

These results show that cationic conductivity along the [001] direction is larger in the bulk crystal than in the domain walls for both temperatures studied. A notable feature in figure 3 is that conductivity in the bulk is only weakly dependent on temperature, but this would not appear to be the case for the walls. This can be understood that within the walls, it is the minimum dimension of the projected aperture on the (001) plane that constitutes the dominant factor in inhibiting mobility along [001]. This is due to the local shear described in the introduction, which has the effect of changing the more circular channel cross-section in the bulk to an (approximately) elliptic one in the walls, resulting in a smaller minimum dimension (the minor axis of the approximate ellipse) in the wall. Indeed, for the 10 K sample depicted in figure 1, the minimum cross-sectional distances measured in the (001) plane are 3.20 Å and 2.73 Å for the bulk and wall channels respectively.

At the higher of the temperatures the cell volume increases (by ∼1.7%) and the tetrahedral arrangement at the walls starts to resemble that in the bulk due to the markedly increased thermal disorder and reduced size of the order parameter. This results in larger channel cross-sections which has the effect of lowering the applied field necessary for promoting ionic conductivity. Hence note that to establish significant ionic mobility on the timescales studied here, the dominant mechanism for causing cationic motion is the value of the applied $\boldsymbol{E}$, rather than any thermal contributions to the cations' kinetic energy.

3.2. Transport along [110]

Quartz also exhibits channels along another direction within the plane of the wall, namely along [110], and our second set of results (figure 4) considers the forced motion of Li^+ ions along this direction.

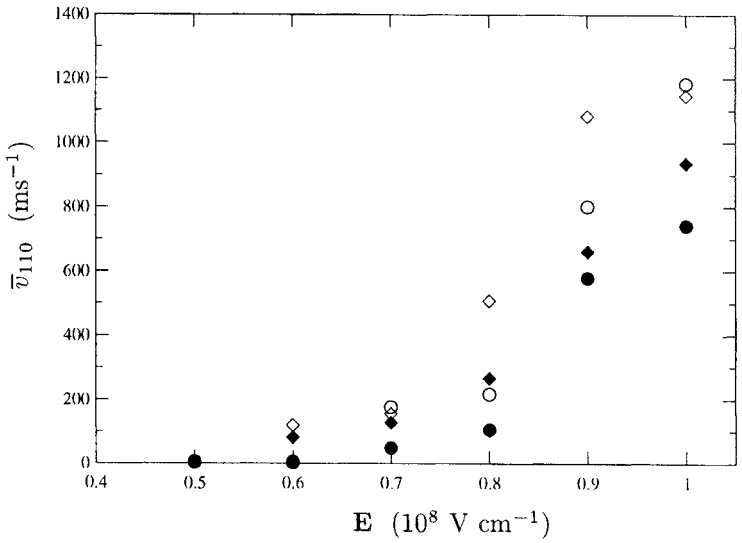

Figure 4. Average velocity along the [110] direction for Li^+ ions with $\boldsymbol{E}$ applied along [110]. Note that circles refer to data at $T = 300$ K while diamonds are for $T = 600$ K; filled symbols are for cations in the bulk while empty symbols are for cations in the walls.

We find that overall conductivity along this direction is poorer than along [001], with a greater applied electric field necessary to promote inter-cavity motion. The second noticeable feature is the greater conductivity within the wall compared to the bulk for both temperatures investigated. This property can again be related to the greater circular cross-section of the superior conducting channel (this time of the wall channels, rather than the bulk). Such behaviour holds for both cations used in this study, with the smaller Li^+ ions being unsurprisingly the more mobile of the two species. A typical trajectory of a Li^+ ion moving in the [110] direction is shown in figure 5. Note that the velocity of the cation is not constant, with an inter-cavity hopping mechanism evident.

3.3. Transport along [100]

The final scenario that we considered has $\boldsymbol{E}$ applied along [100]. This channel is out of the plane of the domain wall, making an angle of 60° with it. We find that pronounced conductivity starts

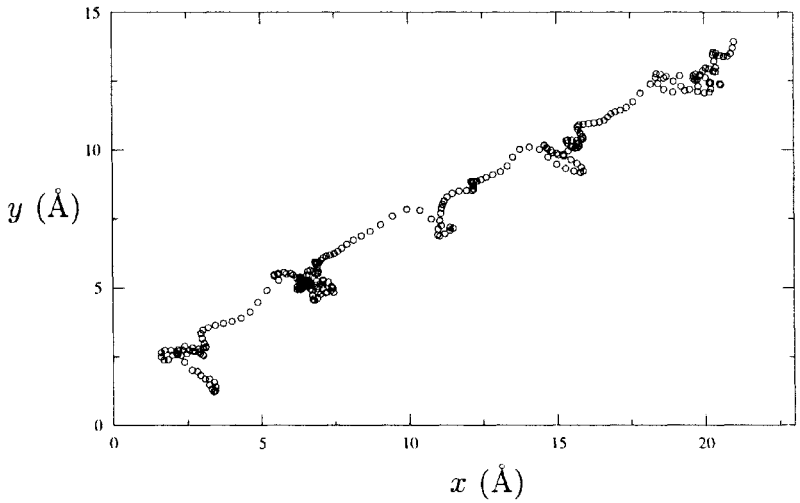

Figure 5. The Li^+-ion trajectory along [110] in a domain wall for a period of 3.75 ps, with $\boldsymbol{E} = 8 \times 10^7$ V cm^{-1}.

at $|\boldsymbol{E}| \sim 8 \times 10^7$ V cm^{-1}, and observe trapping of the cations at the walls provided that $\boldsymbol{E}$ is not too great. This trapping appears to be selective in that only one of the two possible orientations of the wall inhibits the cations' movement. Cations travelling towards a wall along [100] will perceive one of two possible orientations (see figure 6) of the wall, which is due to the shear that creates it. Cations approaching the wall along direction 1 traverse the wall in the same manner as when traversing the bulk, yet those approaching along direction 2 get pinned within the wall. This behaviour persists until a sufficiently strong field ($|\boldsymbol{E}| \sim 1.2 \times 10^8$ V cm^{-1}) is applied which is capable of sweeping the trapped cations out of the wall. However, damage to the crystal starts to become evident at these field strengths.

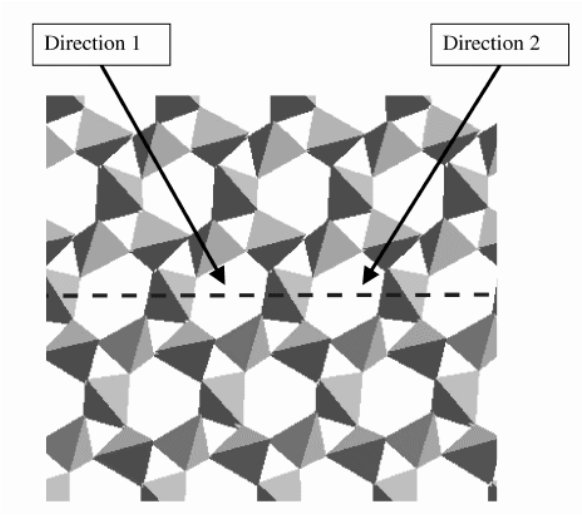

Figure 6. The two possible directions of approach to a wall in the (001) plane.

4. Discussion

In this work we have shown the effects of domain walls in quartz on ionic conductivity. We find that this is not a simple case of two regimes (i.e. bulk and domain wall), but is strongly dependent on the direction of the current within the crystal as may be expected from such an anisotropic crystal. Our first observation is that [001] is the overall superior conducting direction, similar to β-quartz and related alumino-silicates (e.g. β-eucryptite) [32]. That this should be so can be discerned by examining the particle-density distributions for trapped cations: in figure 7 we plot ρ_α, which is the particle density along a cartesian axis α, normalized such that

$$\int_{-\infty}^{\infty} \rho_\alpha(h)\, \mathrm{d}h = 1. \tag{2}$$

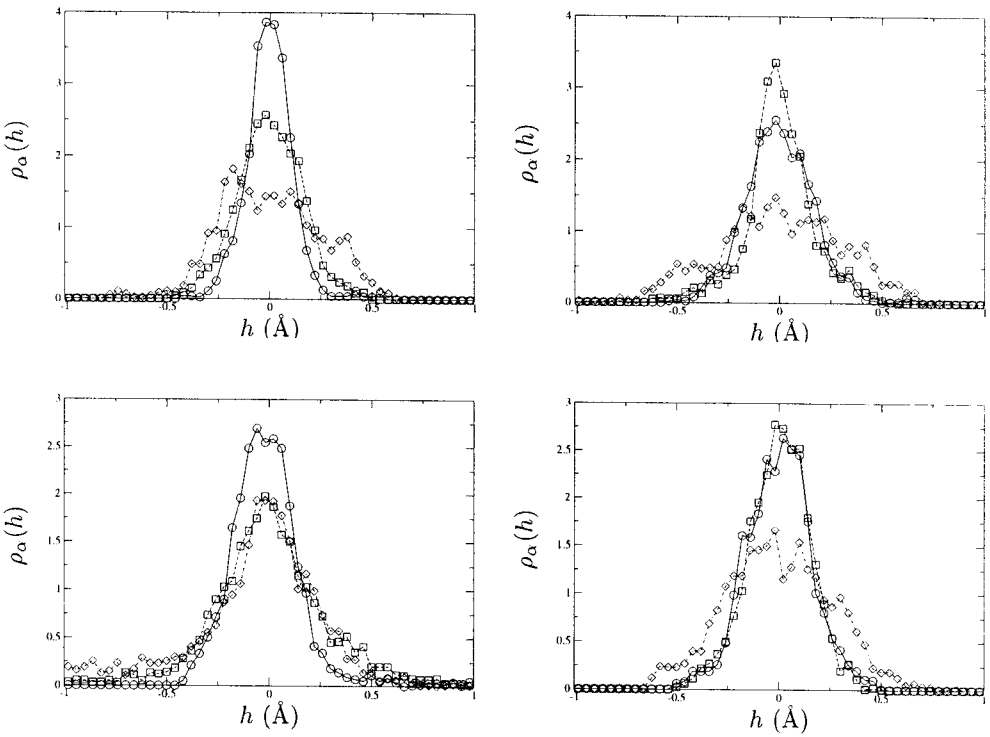

Figure 7. Cation distributions in quartz (see the text). The top two plots are for Na^+ with $\boldsymbol{E} = 0.05$ along [001], while the bottom two plots are for Li^+ with $\boldsymbol{E} = 0.5$ along [110]. Left-hand plots are for ions trapped in the bulk while those on the right are for ions trapped in a wall. Circles, squares and diamonds refer respectively to distributions along the x-, y- and z-axes.

Although an electric field is present in these plots, its strength is not sufficient to induce conductivity over the time span for which the distributions were measured. What is immediately apparent from these graphs is that the cation is least localized along the crystallographic c-axis (which is parallel to the cartesian z-axis).

The new topology of the silica tetrahedral arrangement at a wall can either enhance or reduce ionic transport. This can be attributed to the new closest distance of approach to an oxygen that the cation has to experience in order to channel hop. Increasing this distance reduces the potential barrier experienced by the cation, hence leading to increased conductivity.

The reverse holds for a decreased cation–oxygen distance of approach, resulting in superior bulk conductivity along [001] and wall conductivity along [110].

From the field strengths required to unpin the cations we can extract approximate values of the of the potential barriers that have to be overcome for there to be conductivity at particular temperatures. To do this we assume that the cations sit at the bottom of a potential well at the middle of a cavity and experience the potential maximum when passing into the next cavity. The table below summarizes some values obtained using this simple approach.

Table 3. Unpinning energies required to initiate conductivity.

Cation	Direction	T (K)	E (eV)
Na^+	Bulk [001]	300	0.11
Na^+	Wall [001]	300	0.95
Na^+	Wall [001]	700	0.30
Li^+	Bulk [110]	300	1.55
Li^+	Wall [110]	300	1.44
Li^+	Wall [110]	600	1.37

By comparison, for *correlated* Li^+ diffusion along the c-axis in β-eucryptite, a value of 0.3 eV was obtained from an *ab initio* study by Lichtenstein *et al* [33], although this represents the $T = 0$ K case.

Finally, we find evidence for the trapping of cations on the domain walls when approaching a wall from one of the two possible [100] channels (i.e. from out of the plane of the wall).

Acknowledgments

We are grateful to the High Performance Computing Facility (HPCF) at the University of Cambridge on whose hardware these simulations were performed. MC would like to thank the EPSRC for funding his postdoctoral position, and W Lee and P Dowds for useful discussions.

References

[1] Maier J 1999 *Solid State Phenom.* **67** 45
[2] Borg R J and Dienes G J 1988 *An Introduction to Solid State Diffusion* (New York: Academic)
[3] Salje E K H 2000 *Properties of Complex Inorganic Solids 2* ed A Meike (Dordrecht: Kluwer)
[4] Aird A and Salje E K H 1998 *J. Phys.: Condens. Matter* **10** L337
[5] Aird A and Salje E K H 2000 *Eur. Phys. J.* B **15** 205
[6] Fischer R, Frommeyer G and Schneider A 2001 *Mater. Sci. Eng.* A submitted
[7] Camara F, Doukhan J C and Salje E K H 2000 *Phase Transitions* **71** 227
[8] Hayward S A and Salje E K H 2000 *Mineral. Mag.* **64** 195
[9] Robertson J, Warren W L, Tuttle B A, Dimos D and Smyth D M 1993 *Appl. Phys. Lett.* **63** 1519
[10] Salje E K H 1990 *Phase Transitions in Ferroelastic and Co-Elastic Crystals* (Cambridge: Cambridge University Press)
[11] Semenovskaya S and Khachaturyan A G 1991 *Phys. Rev. Lett.* **67** 2223
[12] Artemev A and Khachaturyan A G 2000 *Mater. Sci. Forum* **327-3** 347
[13] Pertsev N A, Novak J and Salje E K H 2000 *Phil. Mag.* A **80** 2201
[14] Blackburn J F and Salje E K H 1999 *J. Phys.: Condens. Matter* **11** 8477
[15] Salje E K H and Ishibashi Y 1996 *J. Phys.: Condens. Matter* **8** 8477
[16] Novak J and Salje E K H 1998 *J. Phys.: Condens. Matter* **10** L359
[17] Malcherek T, Kroll H and Salje E K H 2000 *Phys. Chem. Minerals* **27** 203
[18] Lemmens H, Czank M, Van Tendeloo G and Amelinckx S 2000 *Phys. Chem. Minerals* **27** 386
[19] Carpenter M A and Salje E K H 1998 *Eur. J. Mineral.* **10** 621
[20] Dolino G 1990 *Phase Transitions* **21** 59

[21] Prívratská J and Janovec V 1999 *Ferroelectrics* **222** 23
[22] Krammer G J, Farragher N P, van Beest B W H and van Santen R A 1991 *Phys. Rev.* B **43** 5068
[23] Forester T R and Smith W 1995 *DL_POLY User Manual* CCLRC, Daresbury Laboratory, Daresbury, Warrington, UK
[24] Kuntzinger S and Ghermani N E 1999 *Acta Crystallogr.* B **55** 273
[25] Gale J D 1998 *2nd Kiel Workshop on the Application of Computer Simulations to Crystallography* DGK
[26] Putnis A 1992 *Introduction to Mineral Sciences* (Cambridge: Cambridge University Press)
[27] Chrosch J and Salje E K H 1999 *J. Appl. Phys.* **85** 722
[28] Houchmanzadeh B, Lajzerowicz J and Salje E 1992 *Phase Transitions* **38** 77
[29] Salje E K H 2000 *Rev. Mineral. Geochem.* **39** 65
[30] Martin J J 1988 *IEEE Trans. Ultrason. Ferroelectr. Freq. Control* **35** 288
[31] Poignon C, Jeandel G and Morlot G 1996 *J. Appl. Phys.* **80** 6192
[32] Haussühl S, Nagel W and Böhm H 1984 *Z. Kristallogr.* **169** 299
[33] Lichtenstein A I, Jones R O, Xu H and Heaney P J 1998 *Phys. Rev.* B **58** 6219